Catalysis Today xxx (xxxx) xxx–xxx

Contents lists available at ScienceDirect

Catalysis Today

journal homepage: www.elsevier.com/locate/cattod

Unusual catalytic activity of TiO_2–$CoTiO_3$ under 1064 nm pulsed laser illumination

Mudit Singh[a,1], Fan Qin[b,1], Olga I. Perez Ordoñez[c,1], Wenli Yang[b], Jiming Bao[d], Arda Genc[e], Viktor G. Hadjiev[f], Francisco C. Robles Hernandez[a,b,d,*]

[a] Department of Mechanical Engineering Technology, University of Houston, Houston, TX, 77204-4020, United States
[b] Materials Science & Engineering, University of Houston, Houston, Texas, 77204, United States
[c] Centro de Investigación en Materiales Avanzados, CIMAV, Chihuahua Mexico, Mexico
[d] Department of Electrical and Computer Engineering, University of Houston, Houston, Texas, 77204, United States
[e] Thermo Fisher Scientific, 5350 NE Dawson Creek Drive, Hillsboro, OR, 97124, United States
[f] Texas Center for Superconductivity, University of Houston, Houston, TX, 77204, United States

ARTICLE INFO

Keywords:
Cobalt titanium oxides
Photocatalysis
Dye degradation
Supercontinuum generation

ABSTRACT

We present the properties of a photo-catalytically activated $CoTiO_3$ framework supported on TiO_2 (rutile). To demonstrate the effectiveness of this TiO_2–$CoTiO_3$ compound under light illumination, we tested its degradation potential against acid orange 7 dye. The dye degradation is effective over a wide range of laser excitation wavelengths from 1064 nm to 532 nm as well as at sunlight simulation conditions. The TiO_2–$CoTiO_3$ compound particles have sizes from 100 nm to a few microns and provide a surprising photocatalytic enhancement under 1064 nm pulsed laser excitation, that is, at photon energies well below the light absorption edge. We attribute the high activity of this material to the interphases between the rutile and $CoTiO_3$ and discuss a number of possible mechanisms for the photocatalytic enhancement under pulsed laser excitations. The dye degradation activity of TiO_2–$CoTiO_3$ increases up to two orders of magnitude when compared to pure TiO_2 or 20at%Co-TiO_2 with TiO_2 in either phases, amorphous or anatase.

1. Introduction

Titanium dioxide (TiO_2) is well known for its photocatalytic properties used for degradation of organics, biological materials, and dyes [1–7]. It is the best catalyst known so far for water splitting [8,9] and used effectively for corrosion protection [10–12]. TiO_2 is commonly found in three different phases known as anatase, rutile, and a little less investigated brookite [13–15]. This polymorphism of TiO_2 is characterized by well-established phase transformation temperatures but in general most of the commercial products are combinations of the above phases. Only carefully synthesized products are single phase; otherwise they are mixtures of 2 or 3 phases. Anatase and rutile have been studied extensively because of their strong photocatalytic activity, but on the downside, both compounds are active only under UV light that limits their applications.

In order a material to be photocatalytically active, the reduction and oxidation energy levels of photocatalytic reactions should lay within the material energy band gap. In addition, the photocatalysis is typically initiated by light excitations with energies higher than that of the band gap. Therefore, the band gap manipulation, including the band edge position [16,17], is of paramount interest in order to produce catalytic materials active under specific light excitations. The band gap manipulation of TiO_2 has demonstrated marginal success on catalytic enhancement using continuous wave (CW) light activation [11,12,15,18,19]. On the other hand, there is not a single report of photocatalysts that are active under pulsed laser excitations with photon energies below the catalyst band gap.

In this paper we present an approach to accomplish higher catalytic activities under 1064 nm pulsed laser illumination using a TiO_2–$CoTiO_3$ photocatalyst.

2. Materials and methods

2.1. Catalyst synthesis

The catalyst precursor, 20at%Co–TiO_2, was prepared as follows:

* Corresponding author at: Department of Mechanical Engineering Technology, University of Houston, Houston, TX, 77204-4020, United States.
E-mail address: fcrobles@uh.edu (F.C. Robles Hernandez).
[1] Authors with equal contribution

https://doi.org/10.1016/j.cattod.2019.06.081
Received 5 February 2019; Received in revised form 5 June 2019; Accepted 28 June 2019
0920-5861/ Published by Elsevier B.V.

Titanium isopropoxide ($Ti[OCH(CH_3)_2]_4$) (150 mL) was added to 200 mL of deionized water during sonication and the entire mixture was subjected to stirring. The sonication was done by using a Misonix S-2000 apparatus delivering 25 J/s. The temperature in the sonicator was kept no higher than 40 °C. The Co is added in the form of CoF. The resulting colloid was dried on a hot plate at 60 °C for 24 h. The dry powders were amorphous mixtures of Co-Ti-O and organic residue. The organic residue was removed by several repeated deionized water washes until the pH was 7. At that point the product was dried again at 60–70 °C and the process was stopped when the powder has a loose appearance (12–15 h). Samples of thus synthesized 20at%Co–TiO_2 were heat treated at 800 °C for 3 h in an electric resistance tube furnace in open-air conditions to produce the TiO_2–$CoTiO_3$ photocatalyst. Pure TiO_2 was synthesized under exact same conditions and serves as a reference sample.

2.2. Characterization

The XRD characterization was conducted on a SIEMENS Diffractometer D5000 equipped with a Cu tube and operated at 40 kV and 30 mA with a corresponding $K\alpha = 0.15406$ nm. Raman spectroscopy was conducted on an XploRA™ apparatus, using a green laser (532 nm) focused on a spot size of 1 μm in diameter. The UV–vis spectra were measure on a Hitachi UV–vis Spectrometer U-2001. The Atomic resolution TEM was carried in a Thermo Fisher Sientific Titan microscope operated at 300 kV with a resolution of approximately 60 pm. The Titan is equipped with Super-X: in-columnEDX system, having 4 SDD detectors integrated into the column solid angle: 0.7-0.9srad.

2.3. Photocatalysis

The catalysts were tested for the degradation of acid orange 7 dye (AO7). In 60 mL of deionized water we maintained an AO7 concentration of 2.10^{-5} M. In each test a given tested photocatalyst in amount of 40 mg was added to the solution followed by sonication for 5 min. The photocatalysis was initiated by light illumination the solution in a flask furnished with a magnetic stirrer. Pulsed laser illumination was provided by a SURELITE – III laser emitting 5 ns pulses with repetition rate 10 Hz at 1064 nm and 532 nm and producing 8 mm diameter laser spot size. Continuous wave (CW) excitations were produced by laser diodes operating at 785 nm and 632 nm. A fluorescent lamp and a Newport Class ABB solar simulator were used as sources for continuous spectra light excitations. The light exposure time was varied from 0 to 180 min. The dye degradation was measured by the changes in UV–vis absorption spectral bands, particularly the one at 485 nm. This spectral band is characteristic for AO7 and corresponds to absorption of the azo-linkage. The equilibrium concentration is calculated as $\%C_e(t) = \frac{C}{C_o}$, where C_o is the initial concentration and C is the one after time t.

3. Results and discussion

3.1. Characterization

The XRD results for the reference TiO_2, 20at%Co–TiO_2, and the heat treated material TiO2–CoTiO3 are presented in Fig. 1a. In this figure one can see that as-synthesized TiO_2 is mostly amorphous. In this case the use of Scherrer method [20,21] to determine the grain size is rather inaccurate. The as-synthesized 20at%Co–TiO_2 sample displays a presence of anatase with the average grain size of 1 nm as determined by Scherrer method. Co additions to any phase of TiO_2 have been reported as an anatase promoter even at lower Co concentrations [11,12,22]. In Fig. 1a the family of XRD reflections of 20at%Co–TiO_2 sample correspond to those of anatase (JCPDS 21–1272), although largely broadened.

The TiO_2–$CoTiO_3$ is highly crystalline with bi-crystal framework composed of organic free rutile and $CoTiO_3$ components. In all cases the respective reflections are well-defined and correspond to XRD JCPDS 88–1175 for TiO_2 (rutile) and JCPDS 77–1373 for ($CoTiO_3$) charts [23,24]. The average grain size of crystals in TiO_2–$CoTiO_3$ is 1.4 μm. This is approximately 3 orders of magnitude larger than the size of crystals found in the as-synthesized 20at%Co–TiO_2 sample. The size of crystals in TiO_2–$CoTiO_3$ is definitely above any quantum confinement threshold that has been reported to be less than 2.5 nm [25–27]. Therefore, the effectiveness of this catalysis is not related to a nanostructured state of material.

The Raman spectra of the samples characterized by XRD are shown in Fig. 1b. By comparing the spectra with those presented in [28], one can conclude that the TiO_2 in as-synthesized TiO_2 and 20at%Co–TiO_2 is anatase as revealed also by XRD. The as-synthesized samples show a well resolved E_g band at 151 cm^{-1}. However, only the 20at%Co–TiO_2 sample shows the expected second E_g band as a shoulder at 199 cm^{-1}. The $3E_g$ modes in anatase are typically observed at 151, 193 and 630 cm^{-1} and those of $2B_{1g}$ and A_{1g} symmetry at 400, 508 and 512 cm^{-1}, respectively [28].

The TiO_2–$CoTiO_3$ sample is mainly composed by a bi-crystal framework of TiO_2 and $CoTiO_3$. The Raman lines of $CoTiO_3$ that crystalizes in the ilmenite structure are reported in [29,30]. The main Raman bands in Fig. 1b for this phase are identified at: 208, 234, 244, 268, 334, 384, 608, and 693 cm^{-1} in agreement with [29,30]. The remaining bands are typical for TiO_2 in the rutile structure (e.g., 142, 234, 364, 432, and 604 cm^{-1}) and compare well with those reported in Refs. [11,12] for rutile. The identification of both phases in TiO_2–$CoTiO_3$ is in agreement with the XRD results.

Fig. 2a compares the Tauc plots of optical absorbance in the as-synthesized TiO_2, 20at%Co–TiO_2, and TiO_2–$CoTiO_3$ samples. The absorption edge of TiO_2 in both as-synthesized samples is comparable to that in our previous findings (2.98–3.09 eV) [10–12] although the 20at%Co–TiO_2 sample exhibits an absorption tail. The corresponding band gap values are close to that in anatase, typically reported as around 3.15 eV [31].

The TiO_2–$CoTiO_3$ sample clearly displays three absorption bands. The first one with band edge at 2.94 eV is attributed to TiO_2 (rutile), in agreement with previous work [32] as well as with the XRD and Raman results in Fig. 1. The other two bands, one at 2.05 eV with the associated cusp at 2.3 eV, are characteristic bands of $CoTiO_3$ as follows from the UV–vis absorption spectra in [33]. The direct band gap in $CoTiO_3$ is at 2.57 eV but it cannot be determined in Fig. 2a because of overlapping with TiO_2 absorption tail. The color of the samples in Fig. 2b-d is in apparent agreement with the absorption measurements thus providing empirical identification of the respective samples.

The degradation sequence is sketched in Fig. 3. From this figure follows that AO7 molecules are expected to degrade into benzene and naphthalene derivatives. The azo-linkage –N = N–, called also azo form, in AO7 molecule, $OH–C_{10}H_6–N=N–C_6H_4–SO_3Na$, ($C_9H_6$ = naphthalene ring, C_6H_4 = benzene ring), has a typical absorption band observed at 430 nm. In hydrated A7O molecules the azo-linkage is in the hydrazone form, $O–C_{10}H_6–N–N<_{H}^{C_6H_4–SO_3Na}$, characterized by absorption band at 485 nm. The UV–vis spectra shown in Fig. 4 indicate that the original AO7 dye in water was in hydrazone form. In Fig. 4a the observed bands at 235 nm and 310 nm are due to absorption of the benzene and naphthalene rings, respectively, in agreement with previous reports [34].

The dye degradation activity, monitored by the intensity of 485 nm absorption band, is displayed in Fig. 4b. It starts immediately and after 90–150 min. the solution was completely decolorized when 97% dye removal was achieved. The decolorization of solution correlates with diminishing of the band at 485 nm in Fig. 4a. The reduction of UV absorption bands at 230 nm and 310 nm shown in Fig. 4c provides evidence for the opening of benzene and naphthalene rings, respectively, with time. Therefore, the degradation of AO7 firstly breaks it

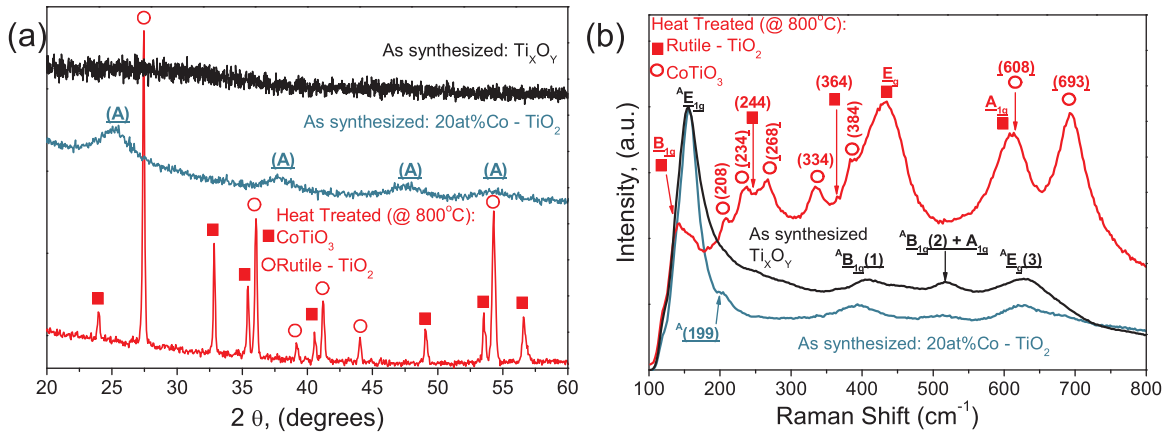

Fig. 1. (a) XRD and (b) Raman characterization of as-synthesized TiXOY reference sample, the raw sample comprising as-synthesized 20at%Co–TiO2 and before and after heat treatment at 800 oC (TiO2–CoTiO3). The label A denotes the characteristic reflections and Raman bands of anatase phase of TiO2.

down benzoic and naphthalene rings that are further degraded to less harmful species.

We note that while the degradation of A07 dye under visible illumination (532 nm) was 97% using TiO_2–$CoTiO_3$ photocatalyst, the corresponding dye degradation on pure TiO_2 under the same conditions resulted in only 1% of dye removal. Therefore, the degradation efficiency of $CoTiO_3$-TiO_2 is two orders of magnitude higher than that of pure TiO_2. The concentration in the degraded dye is closer to the upper limit, often reported in textile effluents and waste waters, for considering it safe.

Fig. 4b also compares the degradation efficiency of TiO_2–$CoTiO_3$ on AO7 dye under 532 nm and 1064 nm laser illuminations. Notably, the degradation under the 1064 nm laser illumination is 97% of the dye in 90 min, whereas that under 532 nm laser the same degree of degradation is achieved in 150 min. On the other hand, the TiO_2 is clearly inactive under both laser irradiations. Fig. 4c shows the degradation of the benzoic and naphthalene rings. Both substances only degrade in the presence of $CoTiO_3$–TiO_2. As expected, the TiO_2 is not active under the laser illuminations used in this work. The analysis for the naphthalene and benzene show 23% and 12% remnants, respectively, under illumination with the 532 nm laser.

In order to present the actual AO7 degradation we plotted a normalized data using the following algorithm (Fig. 4d): $\ln(C_0/C)\bullet I^{-1}$, where C_0, C_e, I are the initial dye concentration, the concentration at the different degradation times, and I is the laser power. Fig. 4d demonstrates that for comparable power of 1064 nm and 532 nm lasers, the 532 nm illumination is more effective for dye degradation.

Fig. 5 shows the TEM and chemical composition analysis, particle morphology, size, and crystalline frameworks of TiO_2–$CoTiO_3$ powder particles. The energy dispersive spectroscopy (EDS) map of a particle, displayed in Fig. 5a, clearly demonstrates the bi-crystal framework of TiO_2–$CoTiO_3$. As per the EDS analysis, the Co concentration in the

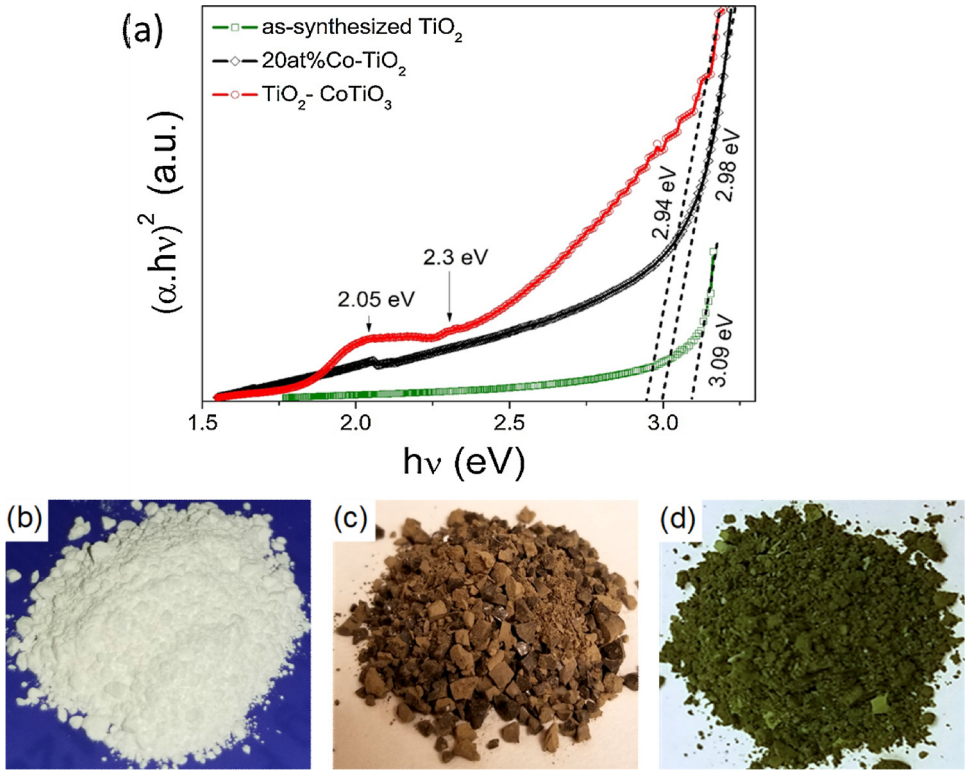

Fig. 2. (a) Tauc plots of experimental absorbance spectra. Pictures of the measured materials: (b) TiO2, (c) 20at%Co-TiO2, (d) TiO2-CoTiO3.

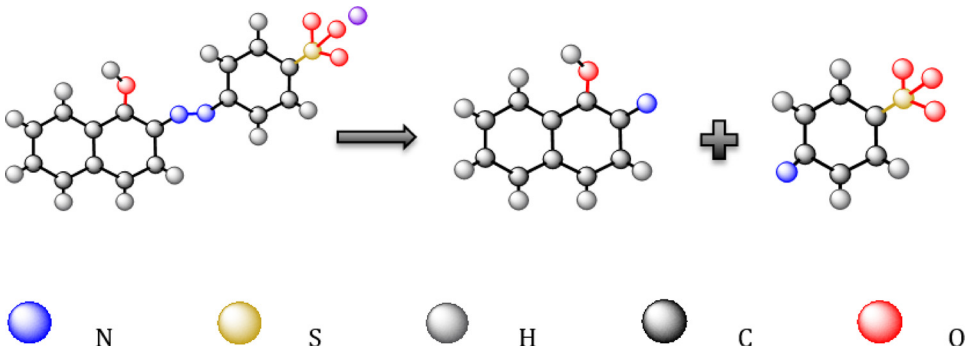

Fig. 3. Sketch of the chemical degradation of Acid Orange 7.

sample is of approximately 10at%Co. The particle size of either phases is clearly above 100 nm, which is in complete agreement with the XRD results. What is even more important is the clear stoichiometric domains for each phase. Fig. 5b displays a sequence of TEM images of two particles joined together. The sequence begins with a lower magnification bright field image that is further magnified to atomic resolution image. The interphase region between the particles is also included along with the corresponding fast Fourier transform (FFT) images. The investigated particles clearly match TiO_2 and $CoTiO_3$ crystal structures. Other images from different locations corresponding to each of the phases are presented in Fig. 5c. The planes and d-spacing shown in Fig. 5c are characteristic only for the identified phases.

One of the most intriguing results reported in this paper is the photocatalytic capability of TiO_2–$CoTiO_3$ under 1064 nm pulsed laser excitation that seems to have no apparent reason to be activated in this compound. As seen in Fig. 2a, TiO_2–$CoTiO_3$ requires a light illumination with wavelengths shorter than 650 nm to activate the electronic band of around 2 eV. As expected, Fig. 6 shows that a 785 nm CW laser

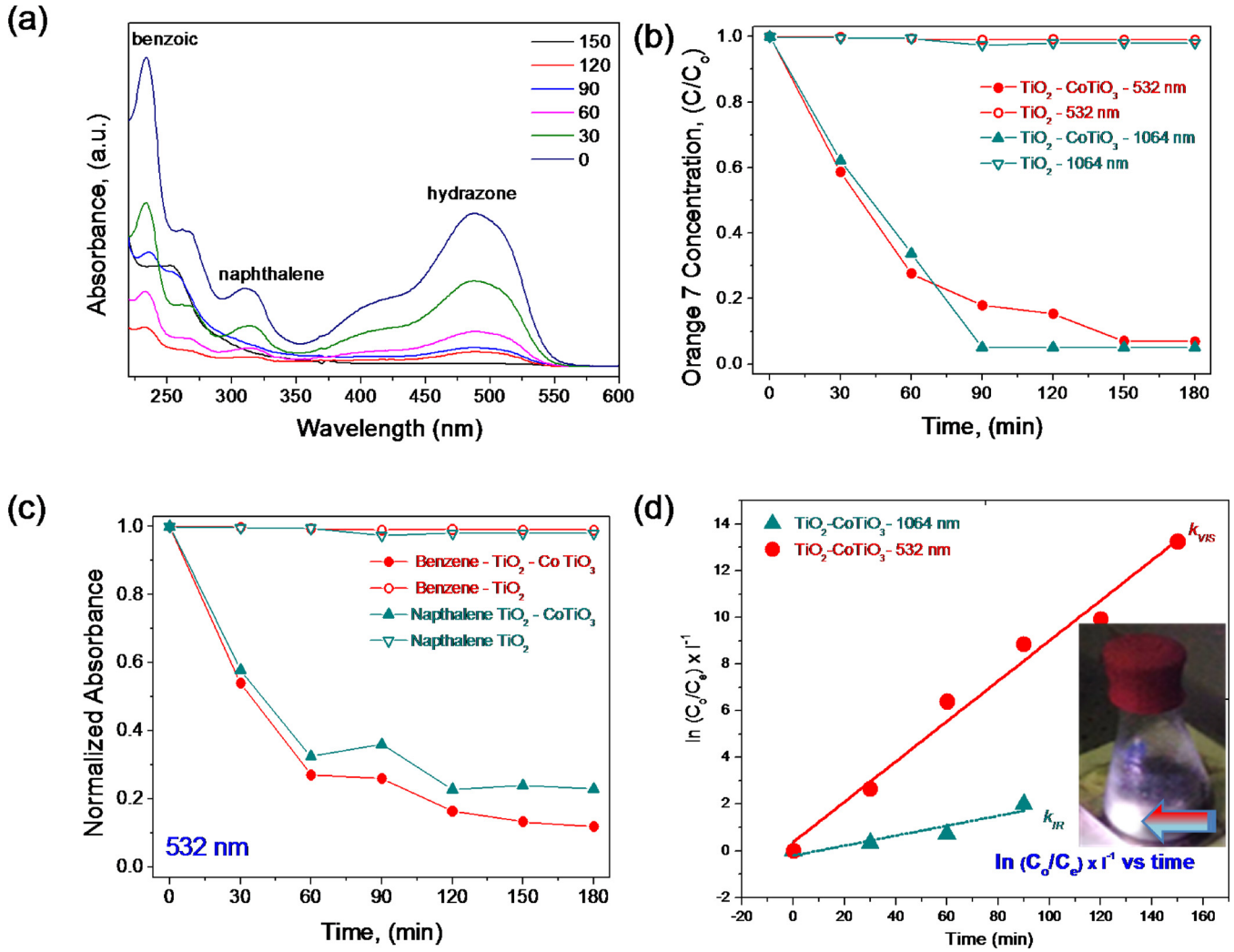

Fig. 4. Photocatalysis results of the degradation of Orange 7 under different wavelength light (532 nm and 1064 nm). (a) UV–vis analysis of the degraded species, (b) concentration of the species during degradation using two laser illuminations, (c) concentration of degraded specie and (d) normalized data. The inset in (d) shows the bright spot produced by 1064 nm pulse laser on TiO2–CoTiO3.

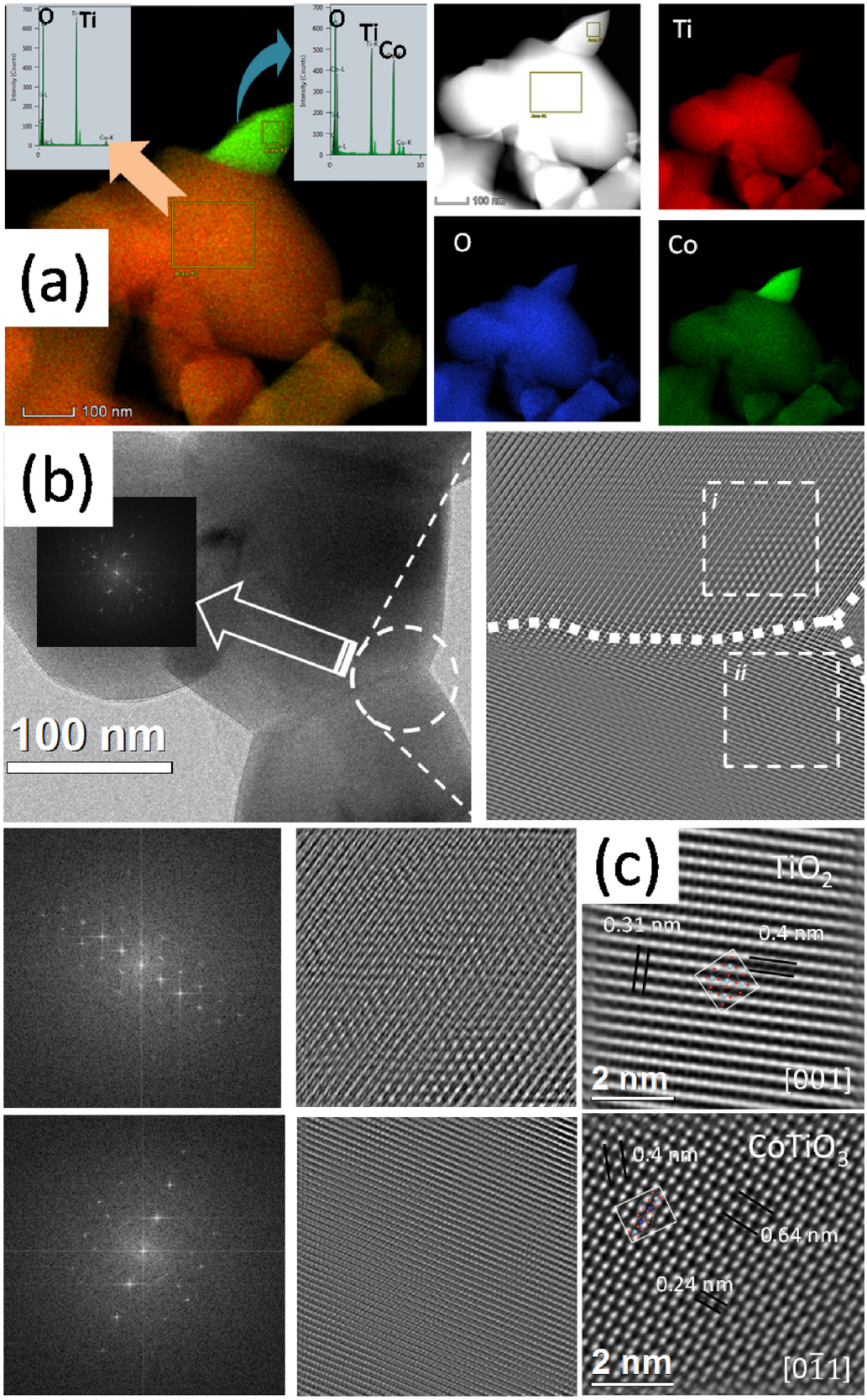

Fig. 5. TEM analysis of the investigated powders. (a) EDS map of a bi-crystal TiO2–CoTiO3, and compositional maps of the same particle, EDS results for areas 1 (TiO2) and 2 (CoTiO3), (b) lower magnification bright field showing the overall particle and the respective aberration corrected HRTEM image revealing the atomic resolution of the bi-crystal frameworks with the FFT for the regions "i" and "ii" and the respective atomic resolution images, and (c) another particle showing its atomic resolution characteristics where it is revealed the crystalline structure for each phase.

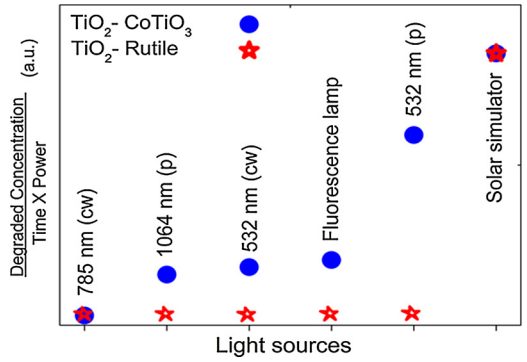

Fig. 6. Dependence of AO7 dye degradation on light excitation sources. (cw): continuous wave laser, (p): pulsed laser.

is incapable of activating photocatalysis in this material.

One the other hand, a pulsed laser operating at 1064 nm (1.165 eV) produces a degradation of AO7 dye as efficiently as that of 532 nm CW laser (Fig. 6). Given that the 1064 nm laser energy is in absorption free energy range for TiO_2–$CoTiO_3$ a number of possible mechanisms can be suggested to explain the observed photocatalytic activation:

The first mechanisms is if TiO_2 and $CoTiO_3$ could create a heterojunction in which the valence band of one of the materials is ˜1.17 eV (1064 nm) below the conduction band of the other one. However, the studies of TiO_2–$CoTiO_3$ heterojunctions show that they are of Type C according to the nomenclature of Ref. [35], that is, both the absolute energies of conduction and valence bands of $CoTiO_3$ are within the band gap of TiO_2 and they cannot produce this effect.

It is also possible that an up-conversion of the 1064 nm laser energy reaches the absorption range of the catalyst through second-harmonic generation (SHG). The SHG is a nonlinear optical effect that is possible only in non-centrosymmetric crystals. Although both TiO_2 and $CoTiO_3$ bulk crystals are centrosymmetric, and therefore SHG intensity is zero, it is well known that strains and crystal boundaries such as crystal faces can break the centrosymmetry and the crystals become SHG active. The SHG generation has been reported at the (110) face of TiO_2 (Rutile) [36] and at the (101) face of anatase [37]. As seen in Fig. 5, TiO_2 in the TiO_2–$CoTiO_3$ catalyst is nanoscale grained with no well-formed crystal faces. On the other hand, $CoTiO_3$ component forms well shaped nanocrystals and it should be the best candidate for SHG in this catalyst. Unfortunately, no reports on SHG at the crystal faces of $CoTiO_3$ were found so far. We believe that SHG at the crystal boundaries of $CoTiO_3$, although expected to be weak, is a viable scenario for explaining the photo activation of the catalyst at 1064 nm. Also, the high peak power in pulsed lasers seems to be of crucial importance. More studies are needed to prove or reject the SHG effect in $CoTiO_3$.

The illumination of TiO_2–$CoTiO_3$ with pulsed laser emission operating at 1064 nm is accompanied by a puzzling phenomenon of generation of white light (see, e.g., Fig. 4d). The secondary white light excitation can provide an alternative explanation for TiO_2–$CoTiO_3$ photocatalytic activation. This effect was not observed in pure $CoTiO_3$ and TiO_2. Since, TiO_2, and/or $CoTiO_3$ are not catalytically active under illumination with visible light, the white light generation has a photocatalytic significance only in the TiO_2–$CoTiO_3$ composite. We measured the temperature at white light spots using combinations of thermocouples, thermometers, and optical pyrometer and in all cases the temperature increase was no more than 1 °C. In addition, we sealed the flask and measured the pressure build up as a potential measure of water evaporation. No measurable pressure change was found either. Therefore, we rule out the possibility of high temperature blackbody radiation and hence thermal decomposition of AO7 dye.

The phenomenon of white light generation in TiO_2–$CoTiO_3$ by pulsed 1064 nm laser illumination is puzzling. One possibility is the generation of supercontinuum (SC). Producing SC in materials is a nonlinear optical effect in which a short laser light pulse broadens its components to SC due to dispersion of the light group velocity [38, 39]. In this case, the 1064 nm laser pulses should fall in the normal dispersion of $CoTiO_3$ in which higher frequencies (shorted wavelength) travels faster that lower frequencies (longer wavelength). This effect can be produced by the third order electric susceptibility of $CoTiO_3$ because its structure is centrosymmetric. Unfortunately, no data on nonlinear optical properties of $CoTiO_3$ has been reported so far in order for one to make assessment of such an effect. In addition, in bulk materials the white light continuum generation is due to the formation of an optical shock at the back of the pump pulses due to space-time focusing and self-steepening [40]. However, if operational, the SC generated in TiO_2–$CoTiO_3$ and extended to near UV can activate TiO_2 component and make the whole composite photocatalytically active.

In summary, all envisaged mechanisms for photocatalytic activities under below the bandgap excitations are based on potential nonlinear optical properties of the specific TiO_2–$CoTiO_3$ composite. The future investigations of this yet unexplained phenomenon will be focused on revealing possible nonlinear optical response in TiO_2–$CoTiO_3$.

4. Conclusions

We have presented a clear evidence that photocatalytically active TiO_2–$CoTiO_3$ is capable of degrading acid orange 7 dye under light illumination with various wavelengths. A laser illumination with photon energies larger than that of the band gaps in TiO_2–$CoTiO_3$ activate the catalytic activity of the material to degrade the investigated dye. We also demonstrate that the 1064 nm laser (1.16 eV) with apparent photon energy below that of the band gaps can activate the TiO_2–$CoTiO_3$ catalytic capabilities provided the light illumination is delivered in short energy pulses. This material reveals a new catalytic mechanism that is neither related to quantum confinement nor to direct photon excitation. We suggest three possible mechanisms to explain the unusual photocatalytic activity of TiO_2–$CoTiO_3$.

Acknowledgements

The authors wish to express their gratitude to Thermo Fisher Scientific and the NanoPort-Portland team for their invaluable support with HRTEM (Dr. D. Gostovic, Dr. L. Pullan, Dr. L Brock and Dr. L. Casalena). VGH work was supported by the State of Texas through the Texas Center for Superconductivity at the University of Houston.

References

[1] L. Yang, S. Luo, Y. Li, Y. Xiao, Q. Kang, Q. Cai, High efficient photocatalytic degradation of p-Nitrophenol on a unique Cu2O/TiO2 p-n heterojunction network catalyst, Environ. Sci. Technol. 44 (2010) 7641–7646.
[2] G.K. Prasad, P.V.R.K. Ramacharyulu, J.P. Kumar, A.R. Srivastava, B. Singh, Photocatalytic degradation of paraoxon-ethyl in aqueous solution using titania nanoparticulate film, Thin Solid Films 520 (2012) 5597–5601.
[3] K. Nagaveni, G. Sivalingam, M.S. Hegde, G. Madras, Photocatalytic degradation of organic compounds over combustion-synthesized Nano-TiO2, Environ. Sci. Technol. 38 (2004) 1600–1604.
[4] B. Kim, D. Kim, D. Cho, S. Cho, Bactericidal effect of TiO2 photocatalyst on selected food-borne pathogenic bacteria, Chemosphere 52 (2003) 277–281.
[5] J. Chen, C.-s. Poon, Photocatalytic construction and building materials: from fundamentals to applications, Build. Environ. 44 (2009) 1899–1906.
[6] J.T. Rajesh, K.S. Praveen, G.K. Ramchandra, V.J. Raksh, Photocatalytic degradation of dyes and organic contaminants in water using nanocrystalline anatase and rutile TiO 2, Sci. Technol. Adv. Mater. 8 (2007) 455.
[7] K. Vinodgopal, D.E. Wynkoop, P.V. Kamat, Environmental photochemistry on semiconductor surfaces: photosensitized degradation of a textile azo dye, acid orange 7, on TiO2 particles using visible light, Environ. Sci. Technol. 30 (1996) 1660–1666.
[8] M. Ni, M.K.H. Leung, D.Y.C. Leung, K. Sumathy, A review and recent developments in photocatalytic water-splitting using TiO2 for hydrogen production, Renewable Sustainable Energy Rev. 11 (2007) 401–425.
[9] S.U.M. Khan, M. Al-Shahry, W.B. Ingler, Efficient photochemical water splitting by a chemically modified n-TiO&sub&2&/sub&gt, Science 297 (2002) 2243.
[10] L. Gonzalez-Reyes, I. Hernández-Pérez, F.C. Robles Hernández, H.D. Rosales, E.M. Arce-Estrada, Sonochemical synthesis of nanostructured anatase and study of

the kinetics among phase transformation and coarsening as a function of heat treatment conditions, J. Eur. Ceram. Soc. 28 (2008) 1585–1594.
[11] A.K.P.D. Savio, J. Fletcher, K. Smith, R. Iyer, J.M. Bao, F.C. Robles Hernández, Environmentally effective photocatalyst CoO–TiO2 synthesized by thermal precipitation of Co in amorphous TiO2, Appl. Catal. B 182 (2016) 449–455.
[12] A.K.P.D. Savio, J. Fletcher, F.C. Robles Hernández, Sonosynthesis of nanostructured TiO2 doped with transition metals having variable bandgap, Ceram. Int. 39 (2013) 2753–2765.
[13] D. Reyes-Coronado, G. Rodríguez-Gattorno, M.E. Espinosa-Pesqueira, C. Cab, Rd. Coss, G. Oskam, Phase-pure TiO 2 nanoparticles: anatase, brookite and rutile, Nanotechnology 19 (2008) 145605.
[14] J.-G. Li, T. Ishigaki, Brookite→rutile phase transformation of TiO2 studied with monodispersed particles, Acta Mater. 52 (2004) 5143–5150.
[15] U. Diebold, The surface science of titanium dioxide, Surf. Sci. Rep. 48 (2003) 53–229.
[16] M. Kuno, J.K. Lee, B.O. Dabbousi, F.V. Mikulec, M.G. Bawendi, The band edge luminescence of surface modified CdSe nanocrystallites: probing the luminescing state, J. Chem. Phys. 106 (1997) 9869–9882.
[17] L. Liao, Q. Zhang, Z. Su, Z. Zhao, Y. Wang, Y. Li, X. Lu, D. Wei, G. Feng, Q. Yu, X. Cai, J. Zhao, Z. Ren, H. Fang, F. Robles-Hernandez, S. Baldelli, J. Bao, Efficient solar water-splitting using a nanocrystalline CoO photocatalyst, Nat. Nanotechnol. 9 (2013) 69.
[18] M.R. Hoffmann, S.T. Martin, W. Choi, D.W. Bahnemann, Environmental applications of semiconductor photocatalysis, Chem. Rev. 95 (1995) 69–96.
[19] M.A. Zanjanchi, H. Noei, M. Moghimi, Rapid determination of aluminum by UV-vis diffuse reflectance spectroscopy with application of suitable adsorbents, Talanta 70 (2006) 933–939.
[20] Z. Zhang, F. Zhou, E.J. Lavernia, On the analysis of grain size in bulk nanocrystalline materials via x-ray diffraction, Metall. Mater. Trans. A 34 (2003) 1349–1355.
[21] H.G. Jiang, M. Rühle, E.J. Lavernia, On the applicability of the x-ray diffraction line profile analysis in extracting grain size and microstrain in nanocrystalline materials, J. Mater. Res. 14 (2011) 549–559.
[22] L. Ming-Wei, G. Xiao-Mei, H. Yin-Ling, W. Cheng-Yang, Characterization of CoTiO3 nanocrystallites prepared by homogeneous precipitation method, J. Nano- Electron. Phys. 5 (2013) 3022-3021.
[23] G.W. Zhou, D.K. Lee, Y.H. Kim, C.W. Kim, Y.S. Kang, Preparation and spectroscopic characterization of ilmenite-type CoTiO3 nanoparticles, Bull. Korean Chem. Soc. 27 (2006) 368–372.
[24] K. Thamaphat, P. Limsuwan, B. Ngotawornchai, Phase Characterization of TiO2 Powder by XRD and TEM\n, (2008).
[25] X. Xue, W. Ji, Z. Mao, H. Mao, Y. Wang, X. Wang, W. Ruan, B. Zhao, J.R. Lombardi, Raman investigation of nanosized TiO2: effect of crystallite size and quantum confinement, J. Phys. Chem. C 116 (2012) 8792–8797.
[26] I. Robel, M. Kuno, P.V. Kamat, Size-dependent Electron injection from excited CdSe quantum dots into TiO2 nanoparticles, J. Am. Chem. Soc. 129 (2007) 4136–4137.
[27] H.W. Peng, J.B. Li, Quantum confinement and electronic properties of rutile TiO2 nanowires, J. Phys. Chem. C 112 (2008) 20241–20245.
[28] U. Balachandran, N.G. Eror, Raman spectra of titanium dioxide, J. Solid State Chem. 42 (1982) 276–282.
[29] M. Shilpy, M.A. Ehsan, T.H. Ali, S.B. Abd Hamid, M.E. Ali, Performance of cobalt titanate towards H2O2 based catalytic oxidation of lignin model compound, RSC Adv. 5 (2015) 79644–79653.
[30] M.A. Ehsan, R. Naeem, H. Khaledi, M. Sohail, A. Hakeem Saeed, M. Mazhar, Fabrication of CoTiO3-TiO2 composite films from a heterobimetallic single source precursor for electrochemical sensing of dopamine, J. Chem. Soc. Dalton Trans. 45 (2016) 10222–10232.
[31] T. Luttrell, S. Halpegamage, J. Tao, A. Kramer, E. Sutter, M. Batzill, Why is anatase a better photocatalyst than rutile? - Model studies on epitaxial TiO2 films, Sci. Rep. 4 (2014) 4043.
[32] M. Landmann, E. Rauls, W.G. Schmidt, The electronic structure and optical response of rutile, anatase and brookite TiO 2, J. Phys. Condens. Matter 24 (2012) 195503.
[33] R. Ye, H. Fang, Y.-Z. Zheng, N. Li, Y. Wang, X. Tao, Fabrication of CoTiO3/g-C3N4 hybrid photocatalysts with enhanced H2 evolution: Z-Scheme photocatalytic mechanism insight, ACS Appl. Mater. Interfaces 8 (2016) 13879–13889.
[34] M. Stylidi, D.I. Kondarides, X.E. Verykios, Visible light-induced photocatalytic degradation of Acid Orange 7 in aqueous TiO2 suspensions, Appl. Catal. B 47 (2004) 189–201.
[35] S.B. Rawal, S. Bera, D. Lee, D.-J. Jang, W.I. Lee, Design of visible-light photocatalysts by coupling of narrow bandgap semiconductors and TiO2: effect of their relative energy band positions on the photocatalytic efficiency, Catal. Sci. Technol. 3 (2013) 1822–1830.
[36] K. Eiichi, M. Goro, U. Sukekatsu, Surface optical second harmonic generation from rutile t i O 2 (110) in air, J. Appl. Phys. 36 (1997) 7250.
[37] S. Nakamura, K. Matsuda, T. Wakasugi, E. Kobayashi, G. Mizutani, S. Ushioda, T. Sekiya, S. Kurita, Optical second-harmonic generation from the anatase TiO2 (101) face, J. Lumin. 87–89 (2000) 862–864.